npj Science of Food

https://doi.org/10.1038/s41538-026-00808-5

Article in Press

Phase change material-based antibacterial nanoparticles for short-term preservation of cooked meat during temperature abuse

Received: 7 August 2025

Accepted: 12 March 2026

Cite this article as: Wu, T., Dong, Y., Zhu, W. *et al.* Phase change material-based antibacterial nanoparticles for short-term preservation of cooked meat during temperature abuse. *npj Sci Food* (2026). https://doi.org/10.1038/s41538-026-00808-5

Tong Wu, Yuhe Dong, Wanying Zhu, Zesen Xie, Tao Jiang, Xi Yu, Ying Xiao, Siyao Sui & Tian Zhong

Phase change material-based antibacterial nanoparticles for short-term preservation of cooked meat during temperature abuse

Tong Wu[a], Yuhe Dong[b], Wanying Zhu[a], Zesen Xie[b], Tao Jiang[b], Xi Yu[b], Ying Xiao[b], Siyao Sui[c], and Tian Zhong[b,d,*]

[a]*Faculty of Chinese Medicine, Macau University of Science and Technology, Macao SAR, China*

[b]*Faculty of Medicine, Macau University of Science and Technology, Macao SAR, China*

[c]*Suzhou Academy of Agricultural Sciences, Suzhou, Jiangsu, China*

[d]*Zhuhai MUST Science and Technology Research Institute, Zhuhai, Guangdong, China*

* Correspondence to: tzhong@must.edu.mo

Abstract

To prevent the rapid microbial growth caused by unintended temperature abuse during the handling of cooked meat, such as malfunctioning hot-holding equipment or improper storage, this study developed a smart formulation that can be triggered by high temperature to release antibacterial agents on demand. A mixture of lauric acid and stearic acid was employed as the phase change material (PCM), and cinnamaldehyde (CA) was used as the active substance to fabricate this composite (CA/PCM). At 42°C, CA/PCM can transit from a solid phase to a molten state, leading to the rapid release of embedded CA. *In vitro* experiments showed that, compared with the 25°C group, the CA/PCM-42°C group reduced the colony counts of *E. coli* and *S. aureus* by 74.5% and 74.0%, respectively, and also decreased the biofilm absorbance by 92.75% and 82.08%, respectively. Compared with the samples stored at 25°C, the inoculated meat stored at 42°C for 24 h exhibited smaller changes in colour ($\Delta E^* < 3.5$), hardness, pH, TVB-N, and MDA values. Moreover, the microbial counts remained below 5 log CFU·g^{-1}. The results demonstrate that CA/PCM serves as an effective fail-safe strategy, providing targeted antimicrobial protection specifically under temperature-abuse conditions for the preservation of cooked meat.

Keywords: on-demand release, controlled release, temperature-responsive, smart packaging

1 Introduction

Cooked meat, due to its high lipid and protein content and elevated water activity, is particularly susceptible to rapid spoilage and quality degradation caused by microbial growth and enzymatic activity[1,2]. To ensure safety and extend shelf-life, commercially available cooked meat products are required to be stored either under refrigeration or maintained hot above 60°C, according to standard food safety practices[3]. However, a significant risk arises from unintended temperature abuse, where equipment malfunction, improper handling, or environmental fluctuations could cause the product temperature to fall into the microbial growth danger zone

(approximately 5-57°C)[3]. Within this range, especially between 40 and 45°C, microbial proliferation accelerates dramatically, posing a critical food safety challenge[4,5].

PCMs are a class of temperature-sensitive materials that change the solid and liquid phases due to temperature changes, which allows them to serve as gates for the intelligent release of active substances[6]. When the temperature is below the melting point of the PCM, active substances are confined within the solid PCM matrix. However, as heat causes the material to change state from solid to liquid, those embedded components freely diffuse and disseminate from the melted medium, forming an antibacterial atmosphere[7]. Therefore, PCM-based composites offer a promising platform for the on-demand release of antimicrobial agents[8]. In recent years, the use of PCMs in food packaging has advanced from providing simple thermal buffering to enabling multifunctional active and smart systems. For example, microencapsulated PCMs have been applied to maintain the quality of products like chocolate, ice cream, and mushrooms by mitigating temperature fluctuations[9,10]. PCMs have also been combined with antimicrobial agents to preserve meat, fruits, vegetables, and seafood. However, in these systems, the release of active compounds typically depends on passive diffusion or matrix degradation, rather than on a precise, phase-change-mediated thermal trigger[11,12]. Therefore, developing eutectic PCMs capable of actively releasing antimicrobial agents via response triggering within specific temperatures, particularly for the preservation of cooked meat, remains an underexplored area. Among various reported PCMs, a eutectic mixture of lauric acid (LA) and stearic acid (SA) at a 4:1 ratio exhibits a melting point near 39°C[13,14], which is a temperature range that coincides with the accelerated growth window of many food-spoilage microorganisms. Importantly, both LA and SA are generally recognized as safe (GRAS) and are widely used as food additives, which supports their suitability for edible packaging applications[15,16].

Among food antimicrobials, cinnamaldehyde (CA) is an organic aldehyde compound found in the genus *Cinnamomum* and is the main active component of cinnamon oil[17]. CA has been approved as a safe food-flavouring agent by the joint FAO/WHO Expert Committee on Food

Additives (JECFA)[18]. Moreover, CA has been reported to have excellent inhibitory efficacy against major foodborne pathogens commonly found in meat, such as *Staphylococcus aureus* (*S. aureus*) and *Escherichia coli* (*E. coli*)[19–21]. However, the direct use of pure CA and direct contact with food are both undesirable because the rapid volatilization of CA leads to the failure of antibacterial activity after a period of time, while its irritating odor and strong reducibility also affect the flavour of food and cause damage to the food surface[22]. To address these challenges, a wide range of biodegradable materials (such as polysaccharides, proteins, and lipids)[23] and encapsulation technologies (including polysaccharide-protein copolymers, microcapsules, inclusion complexes, liposomes, and solid lipid nanoparticles)[24] have been developed for the controlled release of antibacterial agents to meet long-term antibacterial requirements in food preservation. Many of these carriers use food-grade materials, such as lecithin (GRAS) and PEG-6000 (less than 10 mg/kg bw, JECFA), and are commonly used as emulsifiers and stabilizers in food systems[25,26]. They are also added to lipid nanocarriers to improve stability and control release behaviour. Furthermore, more advanced stimulus-responsive strategies have also been devised for on-demand release formulations by utilizing external stimuli (such as temperature fluctuations, humidity variations, pH changes or enzymatic reactions) triggered to induce shell or matrix degradation and subsequent release of antibacterial agents[27,28].

Against this backdrop, this study proposes a novel method for encapsulating CA using a food-grade LA-SA eutectic mixture as a temperature-responsive phase change material (PCM) matrix. This method cleverly targeted the temperature abuse window associated with microbial growth, thereby enabling a targeted smart packaging strategy. In the subsequent study, a PCM-based temperature-responsive nanoparticle (CA/PCM) will be produced to incorporate CA (Figure 1a). At temperatures above 39°C, the nanoparticles are expected to decompose and release antibacterial CA, which inhibits the growth and reproduction of foodborne pathogens on meat (Figure 1b). A complete material characterization will be performed to present the physical and structural properties, particularly its release behaviour and *in vitro* antibacterial activity at diverse temperatures. Furthermore, the CA/PCM nanoparticles will also be applied to cooked meat

pieces for evaluating their ability to inhibit bacterial growth and assessing their impact on quality indicators of meat.

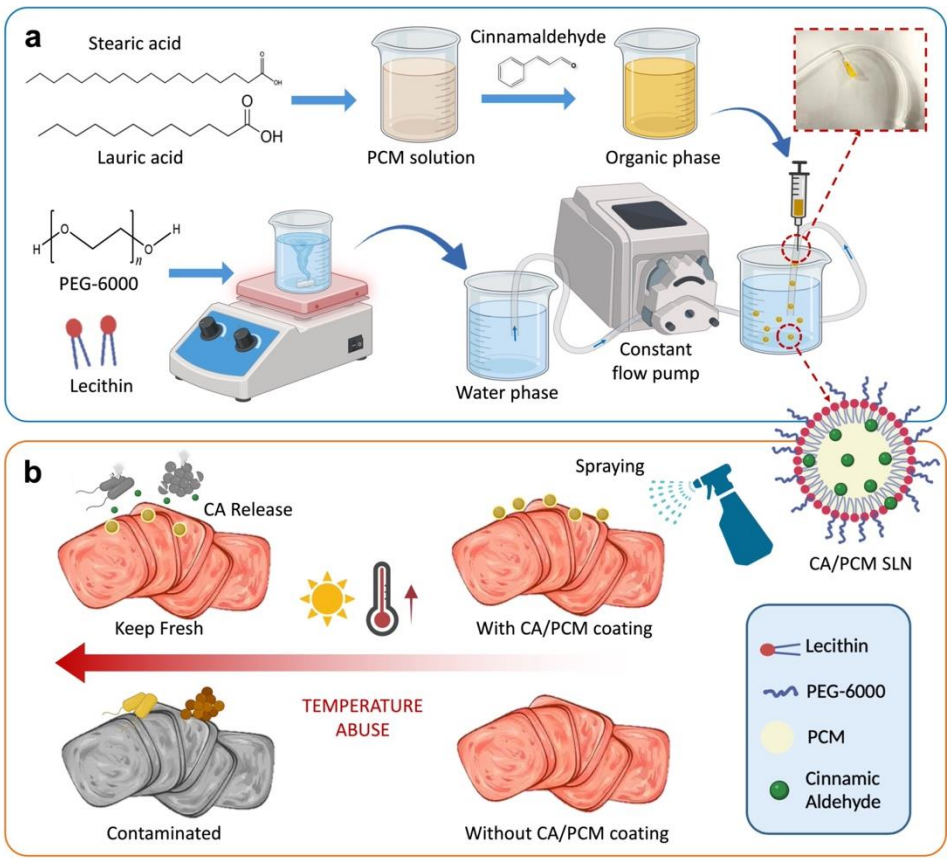

Figure 1. Schematic diagrams of the preparation process for CA/PCM solid lipid nanoparticles (a) and their application in meat preservation (b). PCM: phase-change materials; CA/PCM: phase-change materials loading with cinnamaldehyde. (Schematic created with BioRender.com)

2 Results and discussion

2.1 Characterization

As shown in Figure 2a, freshly prepared emulsions of PCM and CA/PCM exhibited translucency and were white. However, after 7 days at 25°C, the PCM particles without CA tend to aggregate and precipitate at the bottom, resulting in visible stratification. In contrast, the CA/PCM emulsion maintained good dispersion stability over time. This observation indicates the

role of CA in facilitating emulsion dispersion. A previous study reported that CA is a highly reactive compound that can interact with a surfactant/emulsifier at the interface and create a strong network to increase the dispersion of emulsions[24].

The TEM images in Figure 2b demonstrate the core–shell structure of both the PCM and CA/PCM nanoparticles, with the addition of CA resulting in a more regular spherical shape for the PCM nanoparticles. This can be attributed to the molecular affinity and lubrication provided by CA as a lipophilic small molecule in PCM materials composed of SA and LA[29]. Figure 2c shows SEM images of the PCM and CA/PCM samples after drying. The phase change material has a smooth surface texture due to the eutectic mixture of LA-SA, whereas CA/PCM solvent evaporation causes reassembly of the dispersed nanospheres, resulting in an irregular concave-convex morphology.

As shown in Figure 2d and e, the addition of CA increased the average particle size of the PCM nanoparticles from 183 nm to 312.1 nm, whereas the PDI decreased from 0.2504 to 0.1244. These results indicate that the combination of PCM and CA results in more homogeneous and stable nanoparticle systems in the medium, despite the increase in particle size. Zeta potential is also an important factor in indicating particle stability. A value above 30 mV indicates high surface charge repulsion between particles and high particle stability[30,31]. According to Figure 2f, CA/PCM has a larger absolute value of zeta potential (-39.5 ± 0.28 mV) than PCM nanoparticles (- 20.52 ± 0.52 mV), this indicates that the electronegativity of the aldehyde group of CA is adsorbed on the surface of CA/PCM, which increases the negative charge density on the particle surface through the induced charge effect[32]. After the surface charge repulsion force increases, the van der Waals force between particles is less than the electrostatic repulsion force, thus inhibiting particle aggregation and maintaining the stability of nanoparticles[33].

Figure 2g shows that the encapsulation efficiency (EE) and drug loading (DL) values of the nanoparticles are 67.71 ± 2.27% and 65.49 ± 2.41%, respectively, which are within the reasonable ranges (27% - 90%) reported by cinnamaldehyde nanoparticles prepared by antisolvent precipitation[24]. The drug loading is also similar to the results reported by Ma et al. for

encapsulating cinnamaldehyde with lipid nanoparticles and nanoemulsions (54.9%)[34].

Figure 2h shows that PCM nanoparticles do not have a maximum absorption peak above 210 nm, reflecting the characteristic nature of saturated hydrocarbons LA and SA, which are the main constituents of PCM. The CA/PCM nanoparticles exhibit an absorption peak similar to that of CA at approximately 287.9 nm, which is the typical signal for the presence of the aromatic ring. However, the weak intensity of this absorption peak reflects that CA is partially embedded by the PCM.

The TG results (Figure 2i) demonstrate that the residual weight of the pure material decreases to 0 above 200°C. In contrast, CA/PCM presented a more gradual weight loss trend at temperatures less than 400°C. This improved thermal stability might be attributed to the effective encapsulation of CA within the hydrophobic fatty acid matrix (composed of LA, SA, and lecithin). Strong hydrophobic interactions physically restrict the volatility and thermal motion of CA molecules[35]. Furthermore, intermolecular forces such as van der Waals and dipole-dipole interactions between CA and the polar groups (e.g., carboxyl groups) of the fatty acids provide additional stabilization, collectively delaying mass loss during heating[24,36]. This stabilization mechanism aligns with established principles for encapsulating hydrophobic bioactive compounds in lipid-based carriers[37]. The DTG data in Figure 2j show that both thermal decomposition curves reached a maximum rate at approximately 240°C. However, the addition of CA resulted in a smaller peak for CA/PCM, indicating that the incorporation of CA and PCM enhanced the material's thermal stability and reduced the degree of quality degradation. The DSC results (Figure 2k) demonstrate the phase transition of the PCM at 41.25°C due to the melting of the LA-SA eutectic mixture, as well as a small fluctuation at 39.27°C in the curve of CA/PCM, which also indicates the melting of the PCM and the release of CA at this point.

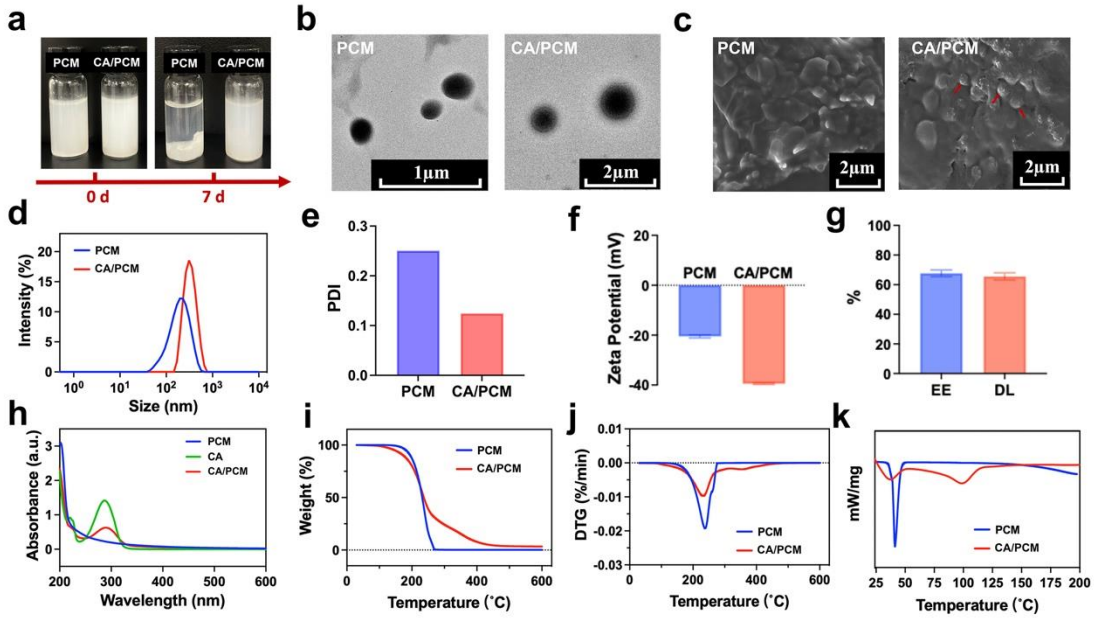

Figure 2. Photographs (a), TEM images (b), SEM images (c), particle size distributions (d), PDIs (e), zeta potentials (f), EEs and DLs (g), UV-vis spectra (h), TG (i), DTG (j), and DSCs (k) of the PCM and CA/PCM nanoparticles. Data are presented as mean ± SD, n = 3.

2.2 Release Behaviour

Figure 3a shows the release progress of CA/PCM nanoparticles in PBS. After 24 h, undissolved white solid samples were still visible in the dialysis bag at 25°C. However, when the dialysis bag was incubated at 42°C, a temperature above the phase transition temperature of the PCM (39°C), it appeared clear and transparent, indicating complete dissolution and penetration of the nanoparticles into the PBS. Upon reaching the phase transition temperature, the material clearly undergoes a solid-liquid transition that dissolves its crystalline state and enhances transparency, fluidity, and solubility, thereby facilitating the migration of small molecules encapsulated in nanoparticles[13,38]. This viewpoint is supported by the cumulative release result of CA presented in Figure 3b. The curve at 25°C remained relatively flat over time, with a final cumulative release percentage of 35.28 ± 1.91% after 4 h. In contrast, the curve at 42°C exhibited an initial burst within the first 30 min and then tended to flatten out, and the 4 h cumulative release rate reached 70.09 ± 3.51%. The cumulative release below 100% could be

attributed to two factors: hydrophobic retention of CA within the lipid matrix and partial evaporation in the open system[35]. This finding is consistent with a previous study that used an LA-SA eutectic mixture for encapsulating hydrophobic drugs, which reported approximately 60% release under similar conditions[39]. Additionally, to further elucidate the impact of temperature stimulation on CA release behaviour, another sample was incubated at 25°C for 2 h followed by switching to 42°C for an additional 2 h. The cumulative release rate significantly increased from 25.19 ± 1.18% to 57.35 ± 3.87% in the first 30 min after the temperature changed and finally stabilized at 73.04 ± 1.14%, which was not significantly different from that observed with constant incubation at 42°C ($P > 0.05$). These findings demonstrate the controlled release capability of CA/PCM nanoparticles in response to temperature.

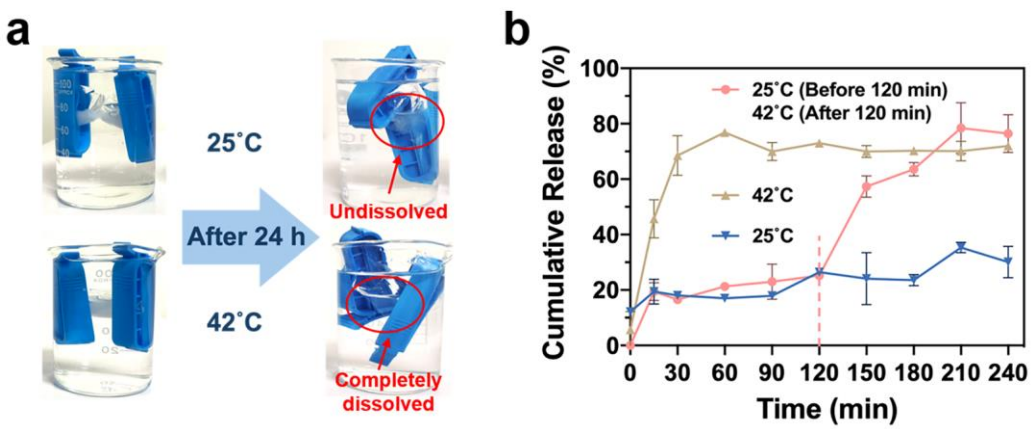

Figure 3. Photographs of CA/PCMs after incubation at 25°C and 42°C for 24 h (a) and the cumulative release rates of CA from CA/PCMs under different conditions: 25°C for 4 h, 42°C for 4 h, and 25°C for 2 h + 42°C for 2 h (b). Data are presented as mean ± SD, n = 3.

2.3 In vitro antibacterial activity

To evaluate the *in vitro* antibacterial activity of the samples against *E. coli* and *S. aureus*, the samples were coincubated with bacteria at two temperatures (25°C and 42°C) for 30 min and then cultured on media for 24 h. Photos and colony count results are presented in Figure 4a and b, respectively. It is well known that the growth rate of microorganisms varies with temperature, but the results in the control group indicate that different temperatures did not induce significant

differences. Similar to those in the control group, the bacterial suspensions cultured at the two temperatures in the PCM group still produced a substantial number of visible colonies on the medium after being diluted 10^8 times, indicating that PCM itself did not have any antibacterial ability. In contrast, pure CA demonstrated strong antibacterial performance regardless of temperature. However, there was no significant difference between CA/PCM and the control at 25°C, but the antibacterial effect was significant at 42°C. After the bacterial suspension was diluted 10^2 times, the colony counts of *E. coli* and *S. aureus* on the agar plates were only 2.40 log and 2.42 log, respectively, which were 74.50% and 74.01% lower than those of the CA/PCM-25°C group (9.31 and 9.26 log, respectively). This reflects the effect of temperature on the antibacterial activity of this stimulus-responsive formulation.

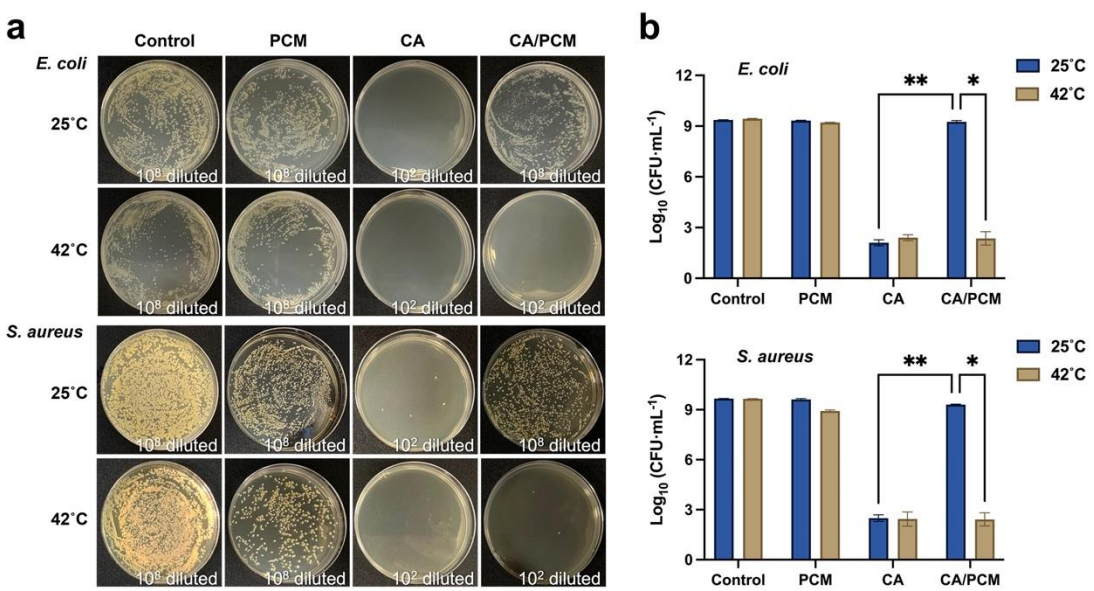

Figure 4. Photographs (a) and counts (b) of colony-forming units (CFUs) of *E. coli* and *S. aureus* coincubated with different samples for 30 min at 25°C and 42°C, followed by culture on agar plates for an additional 24 h at 37°C. Data are presented as mean ± SD, n = 3.

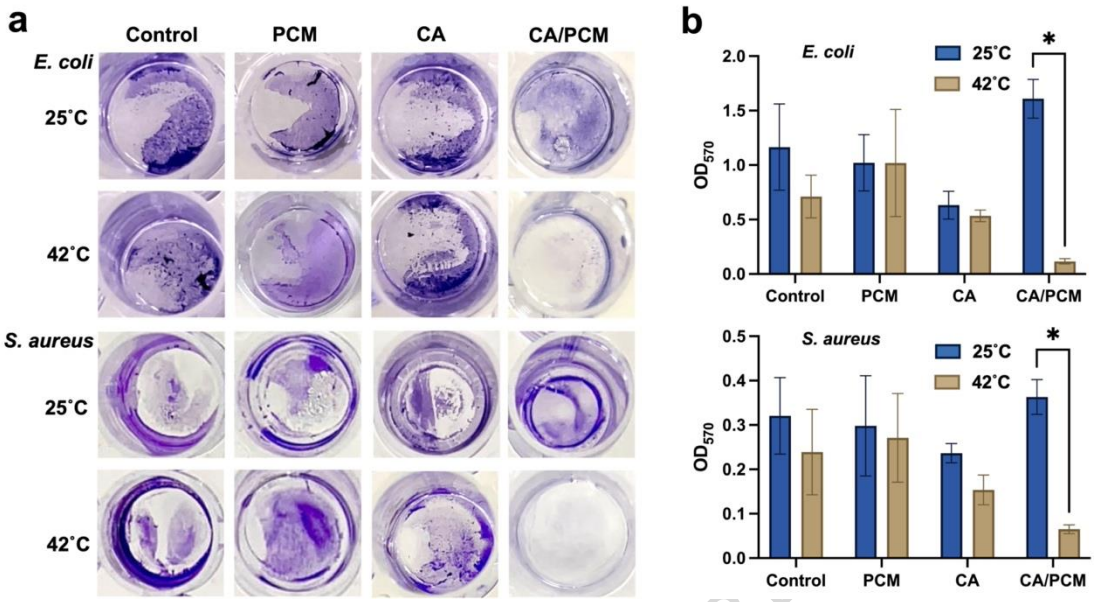

Figure 5. Photographs of crystal violet-stained *E. coli* and *S. aureus* biofilms treated with different samples (a) and OD_{570} values of the biofilm solutions reconstituted with 33% acetic alcohol (in which the *S. aureus* biofilm mixture was diluted 10 times) (b). PBS was used as the control group for each test. Data are presented as mean ± SD, n = 3.

2.4 Biofilm disruption effect

The formation and attachment of bacterial biofilms are major challenges to food safety. Bacterial biofilms act as barriers to prevent bacteriostatic agents from quickly entering cells, making complete elimination of bacteria difficult. In view of the rapid formation of biofilms by *E. coli* and *S. aureus*[40], we used these two bacteria as models to evaluate the clearance effect of CA/PCM on biofilms. Figure 5a and b show crystal violet-stained images of biofilms treated with different solutions (control, pure PCM, free CA and CA/PCM groups) at two temperatures and the absorbance at OD_{570} after reconstitution with 33% acetic alcohol solution. The results revealed no notable difference in biofilm residue between the CA/PCM group and the PCM and control groups at 25°C. At this temperature, the corresponding OD_{570} values for the biofilms of *E. coli* and *S. aureus* were 1.609 ± 0.145 and 0.363 ± 0.032, respectively. In contrast, at 42°C, the biofilms of these two bacteria in the CA/PCM groups were significantly removed, with OD_{570}

values of only 0.117 ± 0.019 and 0.065 ± 0.008, respectively, which were 92.75% and 82.08% lower than those at 25°C. This indicates the key role of temperature in controlling the degradation of CA/PCM. The PCM shell remains solid at 25°C, which provides a strong binding effect for the loaded drug. However, when the temperature increases to 42°C, the PCM shell gradually transforms into a molten state, in which the CA molecules are free to diffuse and volatilize. Moreover, the free CA group did not show satisfactory biofilm removal efficiency, which may be due to the rapid volatilization of CA, resulting in limited interactions with bacteria. In contrast, CA/PCM is degraded under temperature stimulation, and the slowly released CA can extend contact with bacteria, thereby achieving superior biofilm disruption.

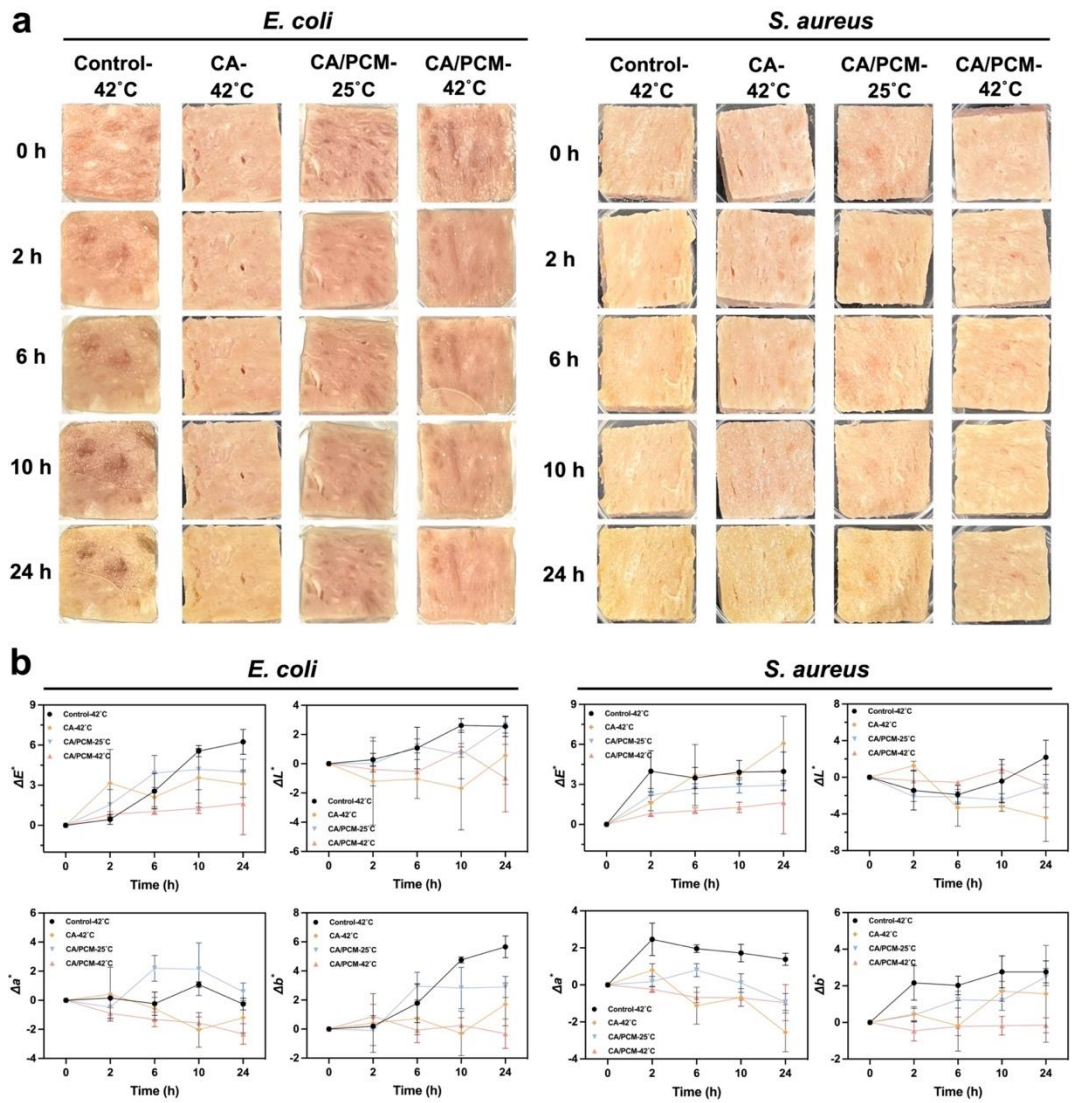

Figure 6. Photographs (a) and colour parameters (b) of meat pieces treated with different samples then inoculated with *E. coli* or *S. aureus* and stored for 24 h. The control-42°C, CA-42°C and CA/PCM-42°C groups were conducted at 42°C, and the CA/PCM-25°C group was conducted at 25°C. Data are presented as mean ± SD, n = 3.

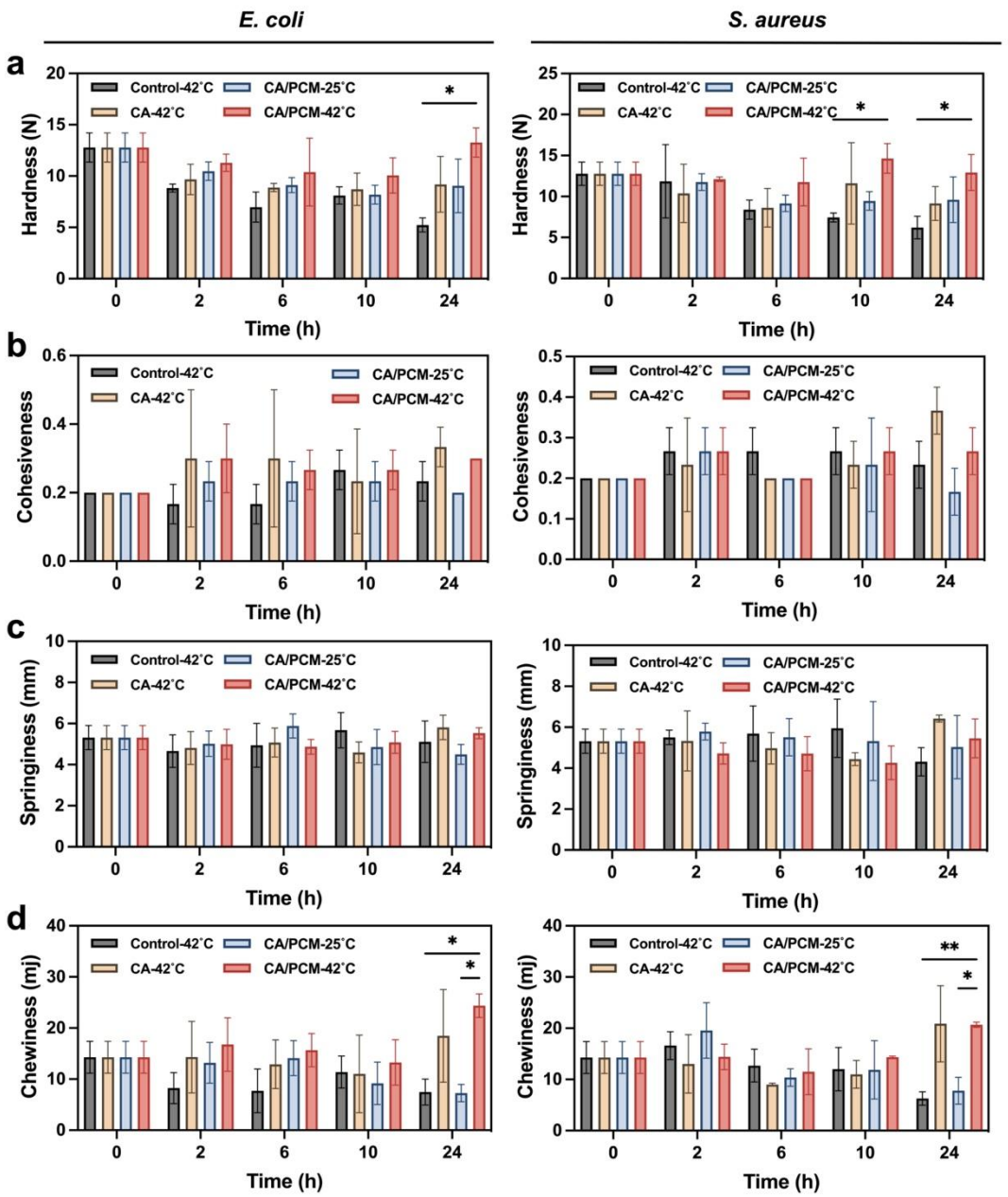

Figure 7. Texture profile analysis in hardness (a), cohesiveness (b), springiness (c), and chewiness (d) of *E. coli*- and *S. aureus*- inoculated meat samples during 24 h of storage. The control-42°C, CA-42°C and CA/PCM-42°C groups were conducted at 42°C, and the CA/PCM-25°C group was conducted at 25°C. Data are presented as mean ± SD, n = 3.

2.5 In vivo evaluation in meat

Figure 6a and b show the morphology and colour changes of meat pieces treated with different

formulas for 24 h. The overall colour differences (ΔE^*) in all the groups tended to increase. According to Mokrzycki and Tatol, when ΔE^* is greater than 3.5, the difference in colour can be significantly noticed; moreover, consumers can judge the decrease in meat freshness through direct observation[41]. After 24 h of incubation at 25°C, the ΔE^* values were 3.97 ± 1.31 and 6.24 ± 0.84 for the groups inoculated with *E. coli* and *S. aureus*, respectively, whereas they were only 1.64 ± 2.09 and 3.07 ± 0.97 for those incubated at 42°C. The greater ΔE^* value in the *S. aureus*-inoculated group may be attributed to the golden appearance of *S. aureus* colonies covering the surface of the meat pieces. In addition, after 24 h of storage, both the Control and the CA/PCM-25°C group showed different degrees of increase in ΔL^* values. This phenomenon is speculated to be due to the hydrolysis of myofibrillar proteins by bacterial proteases, the leakage of cell contents, and the increase in light scattering on the meat surface[41]. The value of Δb^* is a yellow-related indicator and is believed to indicate the degree of lipid peroxidation[42]. Concurrently, bacterial metabolite hydrogen sulphide (H_2S) reacts with myoglobin to form yellow-green sulfmyoglobin, further contributing to elevated b^* values. Accordingly, increased Δb^* values were observed on meat surfaces inoculated with *E. coli* and *S. aureus* in both the Control and CA/PCM-25°C groups after 24 h storage. In contrast, CA/PCM-42°C demonstrated stable ΔL^*, Δa^*, and Δb^* values. On the one hand, the molten PCM forms a hydrophobic barrier on the surface of the meat, reducing the evaporation of moisture from the surface and, to some extent, blocking the contact between the surface of the meat and oxygen, thus delaying the protein denaturation caused by oxidation[43]. On the other hand, this stability reflects the antioxidant and antibacterial effects of CA, wherein its release inhibits myoglobin oxidation and the activity of related proteolytic enzymes, thus maintaining the colour of the meat[44].

Texture properties critically determine consumer acceptability of meat products. Texture profile analysis (Figure 7a) revealed significant hardness reduction in *E. coli*- and *S. aureus*-inoculated meat stored for 24 h in Control and CA/PCM-25°C groups. This textural deterioration stems from microbial protease-mediated degradation of myofibrillar proteins, causing structural denaturation, cross-linking disruption, and fragmentation of the myofibrillar network[45]. In

contrast, CA and CA/PCM-42°C groups maintained hardness integrity, attributable to CA's antimicrobial efficacy in suppressing microbial proliferation and proteolytic activity. While cohesiveness and springiness showed no consistent trends across groups, both CA and CA/PCM-42°C treatments exhibited superior chewiness compared to Control and CA/PCM-25°C groups, demonstrating enhanced textural preservation (Figure 7b - d). The FAO has determined that the maximum acceptable limit for all meat and meat products is 5 logs CFU·g^{-1} [46]. Figure 8a depict changes in total viable counts of *E. coli* and *S. aureus* in cooked meat during 24-h storage. After 24 h, a significant difference ($P < 0.05$) was observed between the CA/PCM-25°C and CA/PCM-42°C groups. The CA/PCM-42°C group exhibited colony counts of 2.98 ± 0.23 log CFU·g^{-1} (*E. coli*) and 4.56 ± 0.09 log CFU·g^{-1} (*S. aureus*), significantly lower than those in the CA/PCM-25°C group (5.10 ± 0.24 log CFU·g^{-1} and 6.03 ± 0.16 log CFU·g^{-1}, respectively). It is noteworthy that the microbial count in the control group stored at 42°C increased rapidly. In contrast, the CA/PCM at the same temperature was significantly inhibited, with all bacterial counts remaining below the FAO limit. This direct comparison demonstrated that the temperature-triggered release of CA in CA/PCM is sufficient to delay meat spoilage at that temperature, validating its role as a rapid-response safety mechanism when necessary.

The pH changes in meats during 24 h of storage are shown in Figure 8b. The initial pH of fresh meat products is generally between 5.5 and 5.8[41]. During 24 h of storage, an overall increasing trend in the control and CA/PCM-25°C groups was observed, which was mainly due to the degradation of meat protein by microorganisms and enzymes and the accumulation of alkaline nitrogen-containing compounds such as ammonia and trimethylamine[47]. Notably, the pH values of *E. coli*- and *S. aureus*-inoculated meat subjected to CA/PCM-42°C treatment were 5.91 ± 0.04 and 5.83 ± 0.07, respectively, which were markedly lower than those of the CA/PCM-25°C groups (6.10 ± 0.03 for *E. coli* and 6.23 ± 0.05 for *S. aureus*). This suggests that the higher temperature (42°C) triggered the release of CA, which may effectively limit the activity of bacteria and enzymes, thereby reducing the production of alkaline nitrogen-containing compounds in protein degradation.

The total volatile salt-based nitrogen (TVB-N) is also an important indicator reflecting the nitrogen-containing substances in meat products. Owing to the degradation of meat protein due to the activity of spoilage microorganisms, volatile alkaline nitrogen-containing substances such as unpleasant ammonia and amines are produced, resulting in an increase in the TVB-N value[48]. While there is no established regulatory TVB-N limit for cooked meat in major food standards, it remains a valuable supplementary indicator of freshness and spoilage progression[49]. Figure 8c shows that after 2 h of storage, the gap between the Control, CA/PCM-25°C and the CA/PCM-42°C group began to increase. After 24 h of storage, the TVB-N values of the *E. coli*- and *S. aureus*-inoculated meat in the CA/PCM-42°C groups were 0.20 ± 0.05 and 0.40 ± 0.05 mg·100 g^{-1}, respectively, which were 67.86% and 47.41% lower than those in the CA/PCM-25°C groups. The results also reflected the antibacterial activity of CA/PCM at 42°C, which significantly suppressed the increase in volatile alkali content caused by enzymes and microorganisms during storage, which is also consistent with the pH results.

Cooked meat products, characterized by high levels of unsaturated fatty acids, are susceptible to lipid peroxidation. Malondialdehyde (MDA), a key by-product of this process, forms a pink chromophore upon reaction with thiobarbituric acid, serving as a reliable biomarker for lipid peroxidation[50]. Figure 8d shows after 24 h of storage, MDA levels in the control group reached 26.43 ± 0.39 nmol·mL^{-1} (*E. coli*) and 7.68 ± 0.19 nmol·mL^{-1} (*S. aureus*), while the CA/PCM-25°C group exhibited values of 21.39 ± 1.87 nmol·mL^{-1} (*E. coli*) and 8.34 ± 0.14 nmol·mL^{-1} (*S. aureus*). In contrast, both the free CA and the CA/PCM-42°C groups maintained significantly lower MDA concentrations, attributable to the radical-scavenging capacity of cinnamaldehyde that mitigates oxidative stress in meat matrices[51]. Critically, CA/PCM stored at 42°C reduced MDA levels by 39.50% (*E. coli*) and 38.41% (*S. aureus*) compared to 25°C ($P < 0.01$), demonstrating its pronounced temperature-responsive release properties.

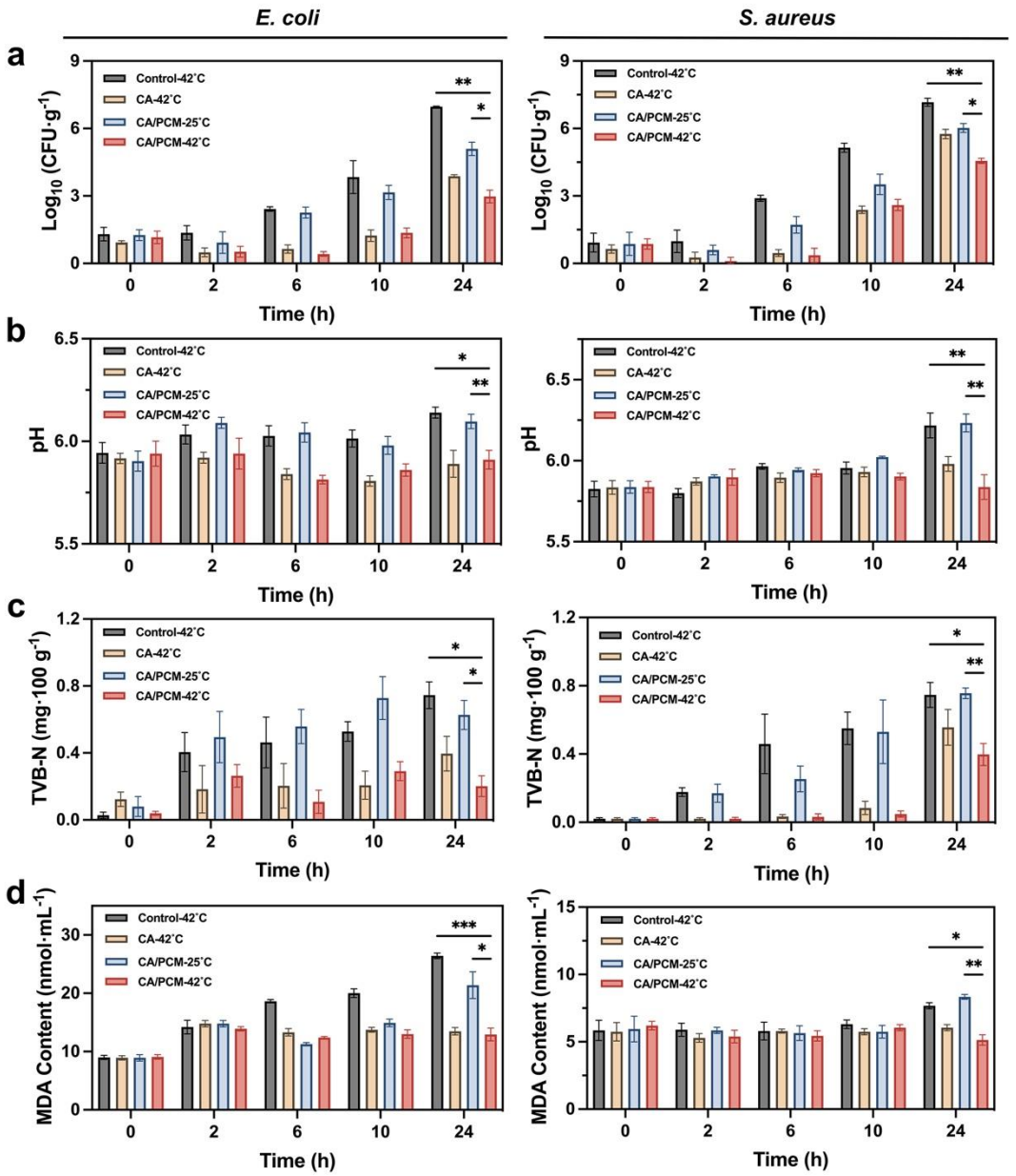

Figure 8. Changes in CFU (a), pH (b), TVB-N (c), and MDA (d) of *E. coli*- and *S. aureus*- inoculated meat samples during 24 h of storage. The control-42°C, CA-42°C and CA/PCM-42°C groups were conducted at 42°C, and the CA/PCM-25°C group was conducted at 25°C. Data are presented as mean ± SD, n = 3.

In this study, we developed a nanoparticle (CA/PCM) by embedding CA as a preservative in a PCM consisting of lauric acid and stearic acid. The characterization results demonstrated that CA/PCM has an obvious spherical core-shell structure with an average particle size of 312.1 nm

and an encapsulation efficiency of 67.71 ± 2.27%. As a temperature-responsive material, a temperature of 42°C can trigger the transition of CA/PCM from a solid phase to a molten state, leading to the rapid release of embedded CA. *In vitro* antibacterial experiments revealed that the colony counts of *E. coli* and *S. aureus* on the agar plates in the CA/PCM-42°C group were 2.40 log and 2.42 log, respectively, which were 74.50% and 74.01% lower than those in the CA/PCM-25°C group (9.31 log and 9.26 log, respectively). The biofilms of both *E. coli* and *S. aureus* were also significantly removed at 42°C, with the absorbance of the reconstituted solution decreasing by 92.75% and 82.08%, respectively, compared with that at 25°C. The bacteria-inoculated meat pieces treated with CA/PCM at 42°C presented significantly less colour change ($\Delta E^* < 3.5$), less change in hardness and lower CFU counts (< 5 log CFU·g^{-1}), pH, TVB-N and MDA values than those treated at 25°C after 24 h. Compared with chemical preservatives and traditional packaging systems, this study provides a condition-responsive and on-demand release antibacterial preservation strategy. This technology can serve as a supplementary measure to traditional preservation techniques to reduce food safety risks in the event of accidental temperature abuse, rather than being a main or routine method of food preservation. Future research should systematically evaluate the long-term (e.g., several months) stability of PCM nanoparticles, especially whether their temperature-responsive release function can be effective in the long term. In addition, it is necessary to study its stability under dynamic temperature cycling and develop PCM formulations that adapt to different trigger temperatures. These are of great value for promoting the application of this technology in practical scenarios.

3 Methods

3.1 Materials

Lauric acid was purchased from Damao Chemical Reagent Factory. Stearic acid was obtained from Shanghai Hushi Laboratory Equipment Co., Ltd. Lecithin was purchased from Aladdin Holdings Group Co., Ltd. Polyethylene glycol-6000 (PEG-6000) was purchased from Cool Chemical Technology (Beijing) Co., Ltd. Cinnamic aldehyde and absolute ethanol were

purchased from Macklin Biochemical Technology Co., Ltd. All reagents used were of analytical grade.

Staphylococcus aureus and *Escherichia coli* were obtained from Guangdong Microbial Culture Collection Centre, China.

3.2 Preparation of CA/PCM

The production of PCM nanoparticles and the encapsulation of CA were performed via antisolvent precipitation, which was adapted from Chen et al.[7]. PCM nanoparticles were produced by passing a PCM solution in ethanol with water through a focused hydrodynamic flow in a homemade fluidic device prepared by mixing. Briefly, a fluidic device was created by inserting a #6 needle (inner diameter of 0.34 mm) into a silicone tube (inner diameter of 2 mm) and fixing it. In the aqueous phase, soybean lecithin and PEG-6000 were dissolved in water to form a lecithin solution with a concentration of 1 $mg \cdot mL^{-1}$. The concentration of the lecithin solution referred to the total concentration of soybean lecithin and PEG-6000, and the ratio of lecithin to PEG-6000 was maintained at 3:1 (*w/w*). A constant flow pump was used to independently control the flow rate of the aqueous phase to stabilize the flow rate at 2.6 $mL \cdot min^{-1}$. The organic phase (the focused phase) was prepared by dissolving LA and SA (4:1 w/w) along with cinnamaldehyde (CA) in ethanol. CA was first dissolved in absolute ethanol to form a 7.5 $mg \cdot mL^{-1}$ stock solution, which was then mixed with the PCM ethanolic solution (5 $mg \cdot mL^{-1}$) at a 1:9 (v/v) ratio, resulting in a final CA concentration of 0.75 $mg \cdot mL^{-1}$ in the organic phase prior to nanoprecipitation. This loading was optimized based on the MIC of CA against the target bacteria (Table S1). The organic phase was injected into the flowing aqueous phase via a syringe at a controlled rate of 0.4 $mL \cdot min^{-1}$. The resulting nanoparticle suspensions were washed three times with water (5 mL per wash) via ultrafiltration tubes (Merck, MWCO 10 kD) centrifuged at 10,000 rpm and 4°C for 20 min per cycle to remove unencapsulated molecules and organic solvents. The resulting nanoparticles were resuspended in 1 mL of water for further use.

3.3 Characterization of CA/PCM

Ultraviolet full-wavelength scanning was analysed via UV-vis spectrophotometer (SHIMADZU, UV-2600i). The size distribution and zeta potential of the PCM nanoparticles were analysed via dynamic light scattering (DLS, ZETASIZER LAB, Malvern) and electrophoretic light scattering (ELS, ZETASIZER LAB, Malvern) at 25°C. The morphology of the PCM nanoparticles was determined by scanning electron microscopy (SEM, JSM-6510, JEOL, Japan) and transmission electron microscopy (TEM, HT7820, Hitachi, Japan). The relationship between the PCM nanoparticle mass and temperature was measured via a thermogravimeter (TG, TA-SDT650, Discovery, USA) and a differential scanning calorimeter (DSC, TA-SDT650, Discovery, USA).

3.4 EE and DL of CA/PCM

The EE and DL of the nanoparticles were determined according to a previously reported[52,53]. The total CA content was obtained by adding anhydrous ethanol to disrupt the structure of the prepared nanoparticles (before washing). Quantification of free CA was achieved by detecting CA in the wash solution from the ultrafiltration tubes. The residual CA/PCM NPs after centrifugation were lyophilized to obtain the weight of nanoparticles. All quantitative detection of CA was performed by measuring absorbance at 287.9 nm via UV-vis. The CA mass concentration was then calculated using a pre-established CA standard curve ($y = 0.3286x - 0.0064$, $r^2 = 0.9996$) in Figure S1. The EE and DL were calculated using the following equation:

$$EE\ (\%) = \frac{CA_{All} - CA_{Free}}{CA_{All}} \times 100 \quad (1)$$

$$DL\ (\%) = \frac{CA_{All} - CA_{Free}}{W} \times 100 \quad (2)$$

where CA_{All} is the total amount of CA (mg), CA_{free} is the amount of free CA (mg), W is the weight of the CA/PCM NPs (mg).

3.5 Temperature-triggered drug release

To determine the release profile of the CA/PCM nanoparticles, the suspension was transferred

to a dialysis bag (Solarbio, MD 25, MWCO 7 kD). Then, the dialysis bags were immersed in a beaker with 100 mL of PBS supplemented with 1% Tween 80 at 25°C and 42°C. At different time points (0, 15, 30, 60, 90, 120, 150, 180, 210, and 240 min), 3 mL aliquots were taken for analysis, followed by the addition of an equivalent volume of dialysis medium. The concentration of CA was determined from the absorbance value measured via a UV spectrophotometer. The formula for calculating the percentage of CA released is referenced from Ouyang et al.[54], and is as follows:

$$Cumulative\ release\ (\%) = \frac{m_n}{m_{drug}} = \frac{[V_1C_n + V_2(C_1 + C_2 + \cdots + C_{n-1})]}{m_{durg}} \times 100 \qquad (3)$$

where m_n represents the cumulative release amount at each time interval (mg), V_1 represents the total volume of the release medium (mL), V_2 is the sampling volume at each time point (mL), C_n is the concentration of cinnamaldehyde in the nth sample (mg·mL^{-1}), and m_{drug} represents the drug input quality (mg).

3.6 Effects on biofilm disruption

The impact of the samples on biofilm disruption was based on previously established protocols[55]. Briefly, Luria-Bertani (LB) medium was used for *E. coli,* and tryptic soy broth (TSB) medium was used for *S. aureus*. The bacteria cultured overnight were diluted to a concentration of 10^8 CFU·mL^{-1} and then cultured at 37°C for 48 h to form a biofilm. Subsequently, 400 μL test samples was added to the biofilm in each well. The test samples were: (1) PBS (control), (2) PCM, (3) free CA (0.48 mg·mL^{-1}), and (4) CA/PCM nanoparticles (CA loading concentration: 0.48 mg·mL^{-1}). The plates were then incubated for an additional 6 h at 25°C or 42°C. After coincubation, the excess liquid was removed, and the residual biofilms were gently washed three times with PBS. Each well containing the biofilms was subsequently stained with 200 μL of 0.1% crystal violet solution for 30 min, the excess dye was subsequently removed, and 400 μL of 33% acetic alcohol solution was added to remove the bound crystal violet from the bacterial biofilms. The absorbance at 570 nm was measured via a microplate reader. All treatments were performed with three technical replicates per experiment, and the

entire assay was independently repeated three times.

3.7 Temperature-responsive antibacterial activity

The antibacterial ability of the nanomaterials was tested using *S. aureus* and *E. coli* in combination with the temperature response. *S. aureus* and *E. coli* were shaken overnight and then diluted to 2×10^8 CFU·mL^{-1}. Subsequently, 300 μL of *S. aureus* or *E. coli* suspension was added to a 1.5 mL Eppendorf tube containing 300 μL of liquid culture medium, PCM, CA/PCM, or CA (equal to the concentration of CA contained in 300 μL of CA/PCM), and the total volume was maintained at 600 μL. The mixed suspension was incubated for one hour at 25°C and 42°C, and then 100 μL of the dilution was spread onto an agar plate. After culturing for 24 h at 37°C, the number of bacterial clones was counted, and the results were expressed as $\log_{10}$ CFU·mL^{-1}.

3.8 In vivo preparation of meat samples and treatments

Commercially cooked Chaoshan-style meat rolls were used as the model food. This product primarily composed of minced pork, starch, and seasonings, is steam-cooked and typically wrapped in food-grade cling film. All samples were purchased on the day of experimentation from ROYAL Supermarket (Macao SAR), transported under refrigeration (4°C) within 30 minutes, and processed immediately. The outer packaging was removed aseptically, and the core portion was cut into uniform cubes (approximately 1.5 × 1.5 × 1.5 cm^3, 5.0 ± 0.2 g). The initial aerobic plate count of the untreated meat was below 10^2 CFU g^{-1}. Meat pieces were allocated into treatment groups.

Meat samples were randomly allocated into three treatment groups: (1) control (saline solution), (2) free CA (0.48 mg·mL^{-1}), and (3) CA/PCM-42°C nanoparticle group (CA loading concentration: 0.48 mg·mL^{-1}). All samples were immersed in their treatment group for 10 min. To simulate a temperature-abuse scenario in which the product core temperature enters the microbial danger zone, all groups were placed in a constant-temperature-humidity incubator set at 42°C. The core temperature was monitored with a probe thermometer and maintained at 42 ±

0.5°C. An additional CA/PCM-25°C group was included, in which meat pieces were not heated and were stored at room temperature (25 ± 0.5°C). Following air-drying, all meat pieces were surface-inoculated with *E. coli* and *S. aureus* at an inoculum level of 10^4 CFU·mL^{-1} in 50 μL per sample and aliquoted into Petri dishes. On Day 0, we prepared all the samples for photography and colorimetric recording at the designated 5 time points (0, 2, 6, 10, and 24 h). Each group contained three pieces of meat from each treatment, and each test was analysed in triplicate. Finally, at every timepoint, the meat samples were homogenized with physiological saline at a mass ratio of 1:10 (w/v) and then subjected to microbiological and chemical analysis.

3.9 Colour

The colorimetric value was determined by the ΔL^* (lightness), Δa^* (redness), and Δb^* (yellowness) of meat, evaluated by a colorimeter (CR-10 Plus, Konica Minolta, Optics, Inc.), which was calibrated by a standard white plate (L^* = 29.7, a^* = - 0.5 and b^* = 0.8). To account for surface heterogeneity, five locations with visually similar colour were randomly selected and marked on each sample on Day 0, these same positions were used for all subsequent measurements throughout the storage period. Colour was measured in triplicate per sample, and the average value was used for analysis.

3.10 Texture profile analysis (TPA)

TPA was evaluated by a texture analyser (TMS-PILOT, Ensoul Tech. Ltd.). In general, three cubes 1.5 cm high and 1.5 cm wide were prepared from every sample. A double compression cycle test was performed up to 50% compression of the original portion height with an acrylic cylinder probe of 3 cm diameter. Force-time deformation curves were obtained by a 100 N sensor, which was triggered at 0.1 N under 1 mm·s^{-1} running speed. The detected parameters were hardness (N), springiness (mm), chewiness (mj), and cohesiveness.

3.11 Total viable counts

A 1 mL suspension was taken from the homogenized sample mixture of each sample for microbial counting under sterile conditions. Total viable counts were examined via the plate counting method on LB agar for *E. coli* and trypticase soy agar medium for *S. aureus* after incubation at 25°C or 42°C for 0, 2, 6, 10, or 24 h. The results are expressed as $\log_{10}$ values ($CFU \cdot g^{-1}$).

3.12 pH value

Each meat block was chopped under sterile conditions and homogenized in 30 mL of normal saline by a homogenizer (FJ-200, Shanghai Huxi Industry Co., Ltd.). The treated sample mixture was allowed to stand for 30 min, and the pH was measured with a pH meter (PHS-3C, Shanghai INESA Scientific Instrument Co., Ltd.) from the supernatant. The measurement was repeated three times for each sample.

3.13 MDA

Lipid oxidation in the samples was assessed by quantifying thiobarbituric acid reactive substances (TBARS), using a commercially available colorimetric diagnostic kit (Nanjing Jiancheng Bioengineering Institute, Nanjing, Jiangsu, China). Following the reaction with thiobarbituric acid, the absorbance of the supernatant was measured spectrophotometrically at 532 nm to determine the amount of MDA. The results are expressed as milligrams of MDA equivalent per kilogram of meat ($nmoL \cdot mL^{-1}$). Each sample was assayed in triplicate.

3.14 TVB-N

TVB-N content of meat was determined via the semimicro Kjeldahl method, and the test procedure was conducted via the national standard method (GB5009.228-2022). Meat homogenate samples (10 mL) pretreated via the pH determination method were mixed with 5 mL of a MgO suspension ($10\ g \cdot L^{-1}$) and subjected to steam distillation. The distillate solution was absorbed with 10 mL H_3BO_3 solution ($20\ g \cdot L^{-1}$) that contained an indicator (methyl red ethanol

solution (1 g·L^{-1}): methylene blue ethanol solution (1 g·L^{-1}) = 2:1). After absorption, the solution was titrated to the end point of purple-red from blue-green, with HCl standard titration solution (0.01 mol·L^{-1}).

The TVB-N values of the samples were calculated via the following formula.

$$TVB-N\ (mg\cdot 100g^{-1}) = \frac{(V_1 - V_2)\times c \times 14}{m \times 10/100} \times 100 \quad (4)$$

where V_1 and V_2 represent the volume of HCl standard solution consumed by the experimental sample and the blank, respectively; c represents the concentration of HCl (mol·L^{-1}); and m represents the mass of each sample.

3.15 Statistical analysis

All the data are expressed as the means ± standard deviations. Analysis of variance was performed on all the data via Graph Pad Prism 9.5.1 software. Two-way ANOVA was used with "treatment" and "temperature"/"time" as factors, including interaction tests. Tukey's post hoc test was used for multiple comparisons. All endpoint data n = 3, and the data met the normality assumption. Differences between different groups at $^{*}P < 0.05$, $^{**}P < 0.01$, and $^{***}P < 0.001$ were considered statistically significant.

Acknowledgements

This study was supported by the Macao FDCT Grants (0005/2024/AGJ and 0009/2023/AFJ) and the Science and Technology Foundation of Suzhou (2022SS25).

Data availability statement

All the data supporting the findings of this study are available within the article and its Supplementary Information files.

Code availability statement

No custom code was used or generated during this study. Statistical analyses were performed using the built-in tools of GraphPad Prism 9.

Declaration of competing interest

None.

Author contributions

Tong Wu: Writing- Original draft, Visualization, Conceptualization, Methodology, Investigation, Data curation. **Yuhe Dong:** Methodology, Investigation, Visualization. **Wanying Zhu:** Investigation, Visualization. **Zesen Xie:** Investigation, Visualization. **Tao Jiang**: Investigation. **Xi Yu:** Writing- Reviewing and Editing. **Ying Xiao:** Writing - review & editing. **Siyao Sui:** Resources. **Tian Zhong:** Writing - review & editing, Conceptualization, Project administration, Supervision.

Reference

1. Dehnad, D., Mirzaei, H., Emam-Djomeh, Z., Jafari, S.-M. & Dadashi, S. Thermal and antimicrobial properties of chitosan–nanocellulose films for extending shelf life of ground meat. *Carbohydrate Polymers* **109**, 148–154 (2014).
2. Rostami, H., Dehnad, D., Jafari, S. M. & Tavakoli, H. R. Evaluation of physical, rheological, microbial, and organoleptic properties of meat powder produced by Refractance Window drying. *Drying Technology* **36**, 1076–1085 (2018).
3. Ricci, A. *et al.* Service temperature preservation approach for food safety: Microbiological evaluation of ready meals. *Food Control* **115**, 107297 (2020).
4. Juneja, V. K. *et al.* A predictive growth model of Staphylococcus aureus during temperature abuse conditions. *Food Research International* **206**, 116032 (2025).
5. Pal, A. & Bhunia, K. Modeling the Biphasic and Monophasic Microbial Growth in Pasteurized Cow Milk Under Isothermal Temperature Abuse. *J Food Process Engineering* **48**, e70064 (2025).
6. Alehosseini, E. & Jafari, S. M. Micro/nano-encapsulated phase change materials (PCMs) as emerging materials for the food industry. *Trends in Food Science & Technology* **91**, 116–128 (2019).
7. Chen, Q. *et al.* Continuous processing of phase-change materials into uniform nanoparticles for near-infrared-triggered drug release. *Nanoscale* **10**, 22312–22318 (2018).
8. Hou, T., Ma, S., Wang, F. & Wang, L. A comprehensive review of intelligent controlled release antimicrobial packaging in food preservation. *Food Sci Biotechnol* **32**, 1459–1478 (2023).
9. Kong, Q. *et al.* Biodegradable phase change materials with high latent heat: Preparation and application on Lentinus edodes storage. *Food Chemistry* **364**, 130391 (2021).
10. Singh, S., Gaikwad, K. K. & Lee, Y. S. Phase change materials for advanced cooling packaging. *Environ Chem Lett* **16**, 845–859 (2018).
11. Karim, M., Fathi, M., Soleimanian-Zad, S. & Spigno, G. Development of sausage packaging with zein nanofibers containing tetradecane produced via needle-less electrospinning method. *Food Packaging and Shelf Life* **33**, 100911 (2022).
12. Nabi, L. & Nourani, M. Biodegradable form stable phase change material for cold storage packaging of meat. *Meat Science* **201**, 109188 (2023).
13. Qiu, J., Huo, D. & Xia, Y. Phase-Change Materials for Controlled Release and Related Applications. *Adv. Mater.* **32**, 2000660 (2020).
14. Zhang, K. *et al.* Nanofibrous hydrogels embedded with phase-change materials: Temperature-responsive dressings for accelerating skin wound healing. *Composites Communications* **25**, 100752 (2021).
15. EFSA Panel on Food Additives and Nutrient Sources added to Food (ANS) *et al.* Re-evaluation of fatty acids (E 570) as a food additive. *EFS2* **15**, (2017).
16. Nitbani, F. O., Tjitda, P. J. P., Nitti, F., Jumina, J. & Detha, A. I. R. Antimicrobial Properties of Lauric Acid and Monolaurin in Virgin Coconut Oil: A Review. *ChemBioEng Reviews* **9**, 442–461 (2022).
17. Chen, H. *et al.* Preparation, characterization, and properties of chitosan films with cinnamaldehyde nanoemulsions. *Food Hydrocolloids* **61**, 662–671 (2016).

18. Abd El-Raouf, O. M., El-Sayed, E.-S. M. & Manie, M. F. Cinnamic Acid and Cinnamaldehyde Ameliorate Cisplatin-Induced Splenotoxicity in Rats: CINNAMIC ACID PREVENTS SPLENOTOXICITY. *J Biochem Mol Toxicol* **29**, 426–431 (2015).
19. He, X. *et al.* Antifungal effect of cinnamic acid and induced resistance of cinnamic acid-protocatechuic acid-CaCl2-NaCl-pullulan composite preservative to Trichoderma harzianum in postharvest Hypsizygus marmoreus. *LWT* **184**, 115108 (2023).
20. Kačániová, M. *et al.* Antimicrobial and antioxidant activities of *Cinnamomum cassia* essential oil and its application in food preservation. *Open Chemistry* **19**, 214–227 (2021).
21. Siddiqua, S., Anusha, B. A., Ashwini, L. S. & Negi, P. S. Antibacterial activity of cinnamaldehyde and clove oil: effect on selected foodborne pathogens in model food systems and watermelon juice. *J Food Sci Technol* **52**, 5834–5841 (2015).
22. Donsì, F. & Ferrari, G. Essential oil nanoemulsions as antimicrobial agents in food. *Journal of Biotechnology* **233**, 106–120 (2016).
23. Yang, S. *et al.* Preparation of cinnamaldehyde-loaded polyhydroxyalkanoate/chitosan porous microspheres with adjustable controlled-release property and its application in fruit preservation. *Food Packaging and Shelf Life* **26**, 100596 (2020).
24. Muhoza, B. *et al.* Encapsulation of cinnamaldehyde: an insight on delivery systems and food applications. *Critical Reviews in Food Science and Nutrition* **63**, 2521–2543 (2023).
25. EFSA Panel on Food Additives and Nutrient Sources added to Food (EFSA ANS Panel) *et al.* Refined exposure assessment of polyethylene glycol (E 1521) from its use as a food additive. *EFS2* **16**, (2018).
26. Gutiérrez-Méndez, N., Chavez-Garay, D. R. & Leal-Ramos, M. Y. Lecithins: A comprehensive review of their properties and their use in formulating microemulsions. *Journal of Food Biochemistry* **46**, (2022).
27. Kardam, S. K., Kadam, A. A. & Dutt, D. Retention of cinnamaldehyde in poly(vinyl alcohol) films intended for preservation of faba beans through vapor-phase antimicrobial effect. *Food Packaging and Shelf Life* **29**, 100704 (2021).
28. Li, Q., Hu, X., Perkins, P. & Ren, T. Antimicrobial film based on poly(lactic acid) and natural halloysite nanotubes for controlled cinnamaldehyde release. *International Journal of Biological Macromolecules* **224**, 848–857 (2023).
29. Friedman, M. Chemistry, Antimicrobial Mechanisms, and Antibiotic Activities of Cinnamaldehyde against Pathogenic Bacteria in Animal Feeds and Human Foods. *J. Agric. Food Chem.* **65**, 10406–10423 (2017).
30. Dong, Y. *et al.* Chitosan-coated liposome with lysozyme-responsive properties for on-demand release of levofloxacin. *International Journal of Biological Macromolecules* **269**, 132271 (2024).
31. Hassane Hamadou, A., Huang, W.-C., Xue, C. & Mao, X. Formulation of vitamin C encapsulation in marine phospholipids nanoliposomes: Characterization and stability evaluation during long term storage. *LWT* **127**, 109439 (2020).
32. Zhang, K. *et al.* Achieving efficient energy utilization by PCM in the food supply chain: Encapsulation technologies, current applications, and future prospects. *Journal of Energy Storage* **79**, 110214 (2024).

33. Lievonen, M. *et al.* A simple process for lignin nanoparticle preparation. *Green Chem.* **18**, 1416–1422 (2016).
34. Ma, F. *et al.* Fucoidan-based cinnamaldehyde nano-emulsion: Fabrication by complex coacervation and application in apple juice. *International Journal of Biological Macromolecules* **315**, 144397 (2025).
35. Chen, W., Cheng, F., Swing, C. J., Xia, S. & Zhang, X. Modulation effect of core-wall ratio on the stability and antibacterial activity of cinnamaldehyde liposomes. *Chemistry and Physics of Lipids* **223**, 104790 (2019).
36. Mura, P. Analytical techniques for characterization of cyclodextrin complexes in the solid state: A review. *Journal of Pharmaceutical and Biomedical Analysis* **113**, 226–238 (2015).
37. McClements, D. J. Nanoemulsions versus microemulsions: terminology, differences, and similarities. *Soft Matter* **8**, 1719–1729 (2012).
38. Zhu, C. *et al.* A Eutectic Mixture of Natural Fatty Acids Can Serve as the Gating Material for Near-Infrared-Triggered Drug Release. *Advanced Materials* **29**, 1703702 (2017).
39. Ghaffari, F. & Shekaari, H. Application of fatty acid-based eutectic mixture as a phase change material in microencapsulation of drugs: preparation, characterization and release behavior. *BMC Chemistry* **19**, 42 (2025).
40. Doyle, A. A. & Stephens, J. C. A review of cinnamaldehyde and its derivatives as antibacterial agents. *Fitoterapia* **139**, 104405 (2019).
41. Ruedt, C., Gibis, M. & Weiss, J. Meat color and iridescence: Origin, analysis, and approaches to modulation. *Comp Rev Food Sci Food Safe* **22**, 3366–3394 (2023).
42. Zhou, Z. Sustained-release antibacterial pads based on nonwovens polyethylene terephthalate modified by β-cyclodextrin embedded with cinnamaldehyde for cold fresh pork preservation. *Food Packaging and Shelf Life* (2020).
43. Bao, Y. & Ertbjerg, P. Effects of protein oxidation on the texture and water-holding of meat: a review. *Critical Reviews in Food Science and Nutrition* **59**, 3564–3578 (2019).
44. Radha Krishnan, K. *et al.* Antimicrobial and antioxidant effects of spice extracts on the shelf life extension of raw chicken meat. *International Journal of Food Microbiology* **171**, 32–40 (2014).
45. Li, K. *et al.* Effect of very fast chilling and aging time on ultra-structure and meat quality characteristics of Chinese Yellow cattle M. Longissimus lumborum. *Meat Science* **92**, 795–804 (2012).
46. Ehsani, A. *et al.* Effect of different types of active biodegradable films containing lactoperoxidase system or sage essential oil on the shelf life of fish burger during refrigerated storage. *LWT* **117**, 108633 (2020).
47. King, D. A., Shackelford, S. D., Rodriguez, A. B. & Wheeler, T. L. Effect of time of measurement on the relationship between metmyoglobin reducing activity and oxygen consumption to instrumental measures of beef longissimus color stability. *Meat Science* **87**, 26–32 (2011).
48. Osanloo, M., Eskandari, Z., Zarenezhad, E., Qasemi, H. & Nematollahi, A. Studying the microbial, chemical, and sensory characteristics of shrimp coated with alginate sodium nanoparticles containing *Zataria multiflora* and *Cuminum cyminum* essential oils. *Food Science &*

Nutrition **11**, 2823–2837 (2023).
49. Bekhit, A. E.-D. A., Holman, B. W. B., Giteru, S. G. & Hopkins, D. L. Total volatile basic nitrogen (TVB-N) and its role in meat spoilage: A review. *Trends in Food Science & Technology* **109**, 280–302 (2021).
50. Kumar, S., Mishra, A. & Pandey, A. K. Antioxidant mediated protective effect of Parthenium hysterophorus against oxidative damage using in vitro models. *BMC Complement Altern Med* **13**, (2013).
51. Sharma, U. K. *et al.* Pharmacological activities of cinnamaldehyde and eugenol: antioxidant, cytotoxic and anti-leishmanial studies. *Cell Mol Biol (Noisy-le-grand)* **63**, 73–78 (2017).
52. Do, N. H. N. *et al.* Novel application of Lemongrass essential Oil-Encapsulated Chitosan nanoparticles as edible coatings for extending the shelf life of strawberries. *Food Measure* **19**, 9020–9031 (2025).
53. Wen, M. M., Abdelwahab, I. A., Aly, R. G. & El-Zahaby, S. A. Nanophyto-gel against multi-drug resistant *Pseudomonas aeruginosa* burn wound infection. *Drug Delivery* **28**, 463–477 (2021).
54. OuYang, Y., Wang, Q., Lou, Y., Song, X. & Wu, M. Smart antibacterial packaging films prepared by TOCNC/CS nanoparticles stabilized Pickering emulsion to prolong shelf-life of fresh pork. *Innovative Food Science & Emerging Technologies* **106**, 104317 (2025).
55. Xiao, Z. *et al.* Trimetallic Nanozyme-Embedded Smart Hydrogel Enables NIR-Controlled Bacterial Killing and Oxidative Stress Alleviation. *Advanced Science* e12875 (2025) doi:10.1002/advs.202512875.